Astron. Astrophys. 355, 552–563 (2000)

ASTRONOMY AND ASTROPHYSICS

A phase-reference study of the quasar pair 1038+528A,B

M.J. Rioja[1,2] **and R.W. Porcas**[3]

[1] Observatorio Astronómico Nacional (OAN), Apartado 1143, 28800 Alcalá de Henares, Spain (rioja@oan.es)
[2] Joint Institute for VLBI in Europe (JIVE), 7990 AA Dwingeloo, The Netherlands
[3] Max-Planck-Institut für Radioastronomie, Auf dem Hügel 69, 53121 Bonn, Germany (porcas@mpifr-bonn.mpg.de)

Received 5 October 1999 / Accepted 20 January 2000

Abstract. We present results from λ 3.6 cm observations of the quasar pair 1038+528 A and B, made in 1995 using the VLBA together with the Effelsberg 100m telescope. We describe the use of a phase-referencing technique to measure the astrometric separation between the quasars. We also introduce a new data analysis method - "hybrid double mapping" - which preserves the relative astrometric information in a single VLBI hybrid map for close source pairs. We combine our measurements with those from three previous epochs, the earliest in 1981. Our new observations confirm the evolution within the structure of quasar B, previously proposed to explain the measured change in the relative separation of the pair. Our upper bound for any systematic proper motion between the mass centres of quasars A and B is 10 μas yr^{-1}. This is set by the limited precision in defining the reference points in the quasars at different epochs and by possible instabilities of the source "core" locations. A separate analysis enables us to put more stringent upper limits to any core motions along the two source axes.

Key words: instrumentation: interferometers – techniques: interferometric – astrometry – radio continuum: general

1. Introduction

The quasar pair 1038+528 A,B (Owen et al. 1978) consists of two flat-spectrum radio sources, with redshifts 0.678 and 2.296 (Owen et al. 1980), separated on the sky by only 33″. This system provides a unique opportunity to carry out high precision, relative astrometric studies using the full precision of VLBI relative phase measurements, since most sources of phase errors are common for the 2 sources (Marcaide & Shapiro 1983).

VLBI studies of the mas-scale structure of flat-spectrum quasars show that they typically have "core-jet" morphologies, consisting of a highly compact feature (the "core") located at the base of an extended linear feature or line of lower brightness components (the "jet"). Both 1038+528 A and B exhibit such structures. In standard models of extragalactic radio sources, these radio-emitting features arise from a collimated beam of plasma which is ejected with a highly relativistic bulk velocity from a region close to a central massive object such as a black hole (see eg. Blandford & Königl 1986). Whilst jet features may correspond to shocks in the moving plasma, and can give rise to the observed "superluminal" component motions in some sources (Porcas 1987), the "core" emission is thought to arise from a more-or-less permanent location close to the origin of the beam, where the ambient conditions correspond to a transition from optically thick to optically thin emission at the observed frequency. Although the "core" position may thus be frequency-dependent, for a fixed observing frequency the core should provide a stable marker, anchored to the central mass of the quasar, whose location can be used to define a precise position for the object as a whole. Although short time-scale variations in physical conditions may cause small changes in the "core" location, over long time-scales it may be used to track any systematic proper motion of the quasar.

The results from a near decade-long VLBI monitoring program on 1038+52A,B at λ 3.6 and 13 cm (from 1981.2 to 1990.5) are reported by Rioja et al. (1997a), whose main conclusions can be summarized as follows:

1. There is no evidence of any relative proper motion between the quasars A and B. The uncertainties in the astrometric parameters result in an upper bound to any systematic relative motion between the cores of 10 μas yr^{-1}, consistent with zero.
2. A compact feature within the jet of quasar B, chosen as the reference point for the structure, expands away from the core at a steady, slow rate of $\sim\ 18\ \pm\ 5\ \mu$as yr^{-1}, corresponding to v=$(0.8 \pm 0.2)\, h^{-1}$ c for a Hubble constant, H_0 = 100 h km s^{-1} Mpc^{-1}; $q_0 = 0.5$. These values are used here throughout.
3. The accuracy of the relative separation measurement is limited by noise and source structure, with estimated precisions of about $50\ \mu$as at λ 3.6 cm at any epoch.
4. Confirmation of the consistently large offset (about 0.7 mas) between the positions of the peak of brightness ("core") at λ 3.6 and 13 cm in quasar A.

New VLBI observations of this pair were made in November 1995 (1995.9) at λ 2, 3.6 and 13 cm. In this paper we report on results from our analysis of the 3.6 cm observations and investigate the temporal evolution of the source structures and relative separation from all four epochs spanning ~ 15 years. Investi-

Send offprint requests to: María J. Rioja

gations of frequency-dependent source structure have also been made from a comparison of the astrometric measurements of the separations between A and B at all 3 wavelengths observed in 1995; these will be presented elsewhere (Rioja & Porcas in preparation).

Our new observations are described in Sect. 2. In Sect. 3 we describe the data reduction and mapping techniques used, and in Sect. 4 an analysis of the measurements in the maps. In Sect. 5 we compare the astrometric results from these observations with those from previous epochs and analyse the changes in separation. Conclusions are presented in Sect. 6.

2. Observations

The pair of radio sources 1038+528 A and B was observed with the NRAO Very Long Baseline Array (VLBA) on November 10, 1995, for a total of 13 hours, alternating every 13 minutes between observations in dual 3.6/13 cm mode and observations at 2 cm. The 100m telescope at Effelsberg was also included in the array for the 3.6/13 cm scans. The primary beamwidths of all the antennas were sufficiently large that both sources could be observed simultaneously at all wavelengths. Each 10 minute observation of 1038+52A,B was preceded by a 3 minute observation of the compact calibration source 0917+624, to monitor the behaviour of the array.

All stations used VLBA terminals to record an aggregate of 64 MHz bandwidth for each scan, using 1-bit sampling, subdivided into 8 channels (mode 128-8-1). For the dual 3.6/13 cm scans, four 8-MHz channels were recorded for each band (2254.5–2286.5 MHz; 8404.5–8436.5 MHz), using RHC polarisation. At 2 cm, eight 8-MHz channels (15 331.5–15 395.5 MHz) were recorded in LHC polarisation.

The correlation was made at the VLBA correlator in Socorro (New Mexico). As for previous epochs, two separate "passes" were needed, using different field centres for the two sources, to recover data for both the A and B quasars from the single observation. Output data sets were generated for the two sources, consisting of the visibility functions averaged to 2 s, with samples every 1 MHz in frequency across the bands.

3. Data reduction

We used the NRAO AIPS package for the data reduction. We applied standard fringe-fitting, amplitude and phase (self-) calibration techniques and produced hybrid maps of each quasar. The astrometric analysis was done using two different mapping methods: a "standard" phase-referencing approach, transferring phase solutions from one quasar to the other (see e.g. Alef 1988; Beasley & Conway 1995) and a novel mapping method for astrometry of close pairs of sources, hybrid double mapping (HDM) (Porcas & Rioja 1996). Both routes preserve the signature of the relative separation of the source pair present in the calibrated phases. These analysis paths are described in Sects. 3.1 to 3.3 below.

3.1. Hybrid mapping in AIPS

We applied standard VLBI hybrid mapping techniques in AIPS for the analysis of the observations of both quasars A and B. We used the information on system temperature, gain curves and telescope gains measured at the individual array elements, to calibrate the raw correlation coefficients. We used the AIPS task FRING to estimate residual antenna-based phases and phase derivatives (delay and rate) at intervals of a few minutes. It is important to realise that FRING is a global self-calibration algorithm, and performs an initial phase self-calibration also. We ran FRING on the A quasar data set, with a point-source input model.

Anticipating our phase-referencing scheme (Sect. 3.2) we applied the antenna phase, delay and rate solutions from A to both the A and B data sets, and averaged them in time to 60 s, and over the total observed bandwidth of 32 MHz. After suitable editing of the data, we made hybrid maps of both quasars, using a number of iterations of a cycle including the mapping task MX and further phase self-calibration with CALIB.

Fig. 1a and b show the hybrid maps for both sources at 3.6 cm in 1995.9. The maps are made using uniform weighting of the visibilities, a map cell size of 0.15 mas and a circular CLEAN restoring beam of 0.5 mas (these same mapping parameters are used throughout this work). The "dirty" beam has a central peak of 0.57 x 0.47 mas in PA -29° (PA = position angle, defined starting at North, increasing through East). The root-mean-square (rms) levels in the A and B maps, in regions away from the source structures (estimated using AIPS task IMSTAT) are 1.0 and 0.12 mJy/beam respectively, an indication that dynamic range considerations dominate over thermal noise in determining the map noise levels.

3.2. Phase referencing in AIPS

In order to make an astrometric estimate of the separation between quasars A and B at this 4th epoch, we first used a "conventional" phase-reference technique to make maps of the quasars which preserve the relative phase information. In practice this consists of using the antenna-based residual terms derived from the analysis of the data of one "reference" source (A), to calibrate the data from simultaneous observations of the other "target" source (B). The reference quasar source structure must first be estimated from a hybrid map, and then fed back into the phase self-calibration process to produce estimates of the antenna-based residuals, free from contamination by source structure.

Phase referencing techniques work under the assumption that the angular separation between the reference and target sources is smaller than the isoplanatic patch size (i.e. the effects of unmodelled perturbations, introduced by the propagation medium, on the observed phases of both sources are not very different) and that any instrumental terms are common. Geometric errors in the correlator model must also be negligible.

Assuming that the antenna residuals have been "cleanly" estimated using the reference source data, the calibrated phases

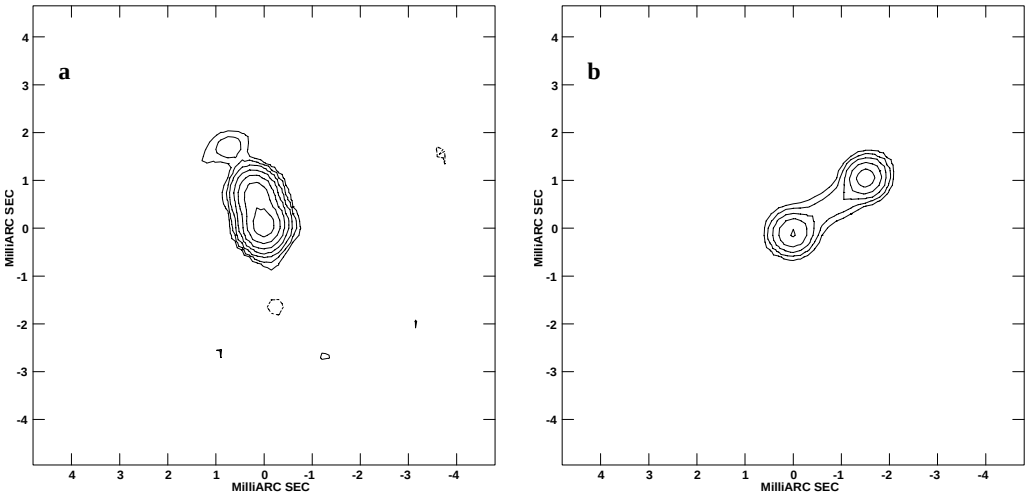

Fig. 1a and b. VLBI hybrid maps of 1038+528 at 3.6 cm. Uniform weighting, CLEAN beam 0.5 x 0.5 mas, pixel size 0.15 mas, tick interval 1 mas. **a** Quasar A. Contours at 3,6,12,24... mJy/beam. **b** Quasar B. Contours at 1.5,3,6,12... mJy/beam.

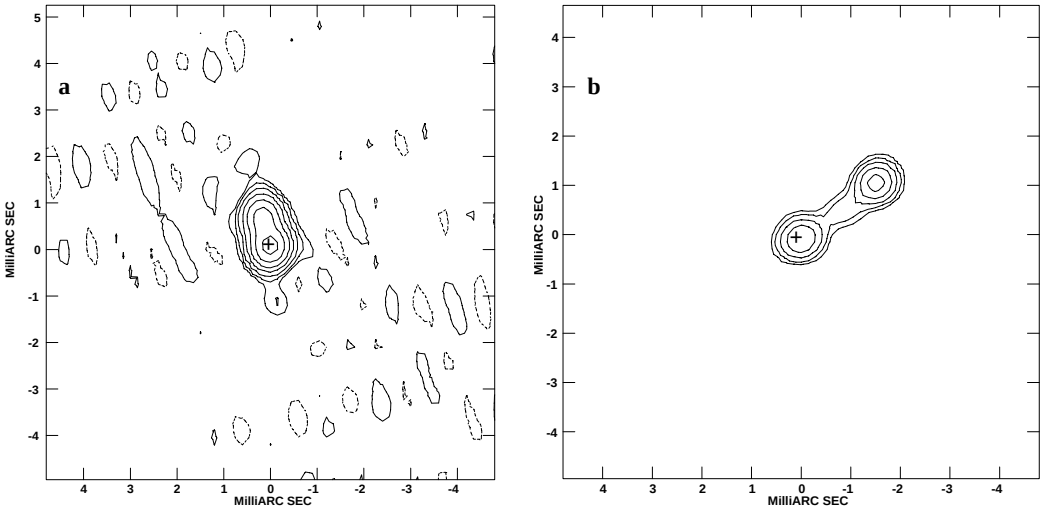

Fig. 2a and b. VLBI phase-reference astrometry maps. Map parameters as in Fig. 1. Astrometry reference points are indicated with a cross. **a** Quasar A. Contours at 3.5,7,14,28... mJy beam^{-1}. **b** Quasar B. Contours at 1.5,3,6,12... mJy beam^{-1}.

of the target source should be free from the errors mentioned above, but still retain the desired signature of the source structure and relative position contributions. The Fourier Transformation of the calibrated visibility function of the target source produces a "phase referenced" map. The offset of the brightness distribution from the centre of this map reflects any error in the assumed relative separation in the correlator model. If the reference source has a true "point" structure and is at the centre of its hybrid map, this offset will be equal to the error; more generally, one should also measure the offset of a reference point in the reference source map, and estimate the error in the source separation used in the correlator model from the difference between the target and reference source offsets.

In general, the success of the phase-referencing technique is critically dependent on the angular separation of the target and reference sources. Simultaneous observation of the sources, as was possible here, significantly simplifies the procedure, eliminates the need for temporal interpolation, and reduces the propagation of errors introduced in the analysis. While random errors increase the noise level in the phase referenced map, systematic errors may bias the estimated angular separation.

For our implementation of phase-referencing using AIPS, we chose to re-FRING the (calibrated) A data set, using our hybrid map of quasar A as an input model, and applied the adjustments to the antenna phase, delay and rate solutions to both the A and B data sets before re-averaging. We then made maps of both A and B using MX, performing no further phase self-calibration. These are our "phase-reference astrometry" (PRA) maps (shown in Fig. 2a and b) on which we performed astrometric measurements (see Sect. 4.2). Although the rms noise levels in the PRA maps are slightly higher than in the corresponding hybrid maps (2.0 mJy beam^{-1} for A and 0.24 mJy beam^{-1} for B), our procedure ensures that the A and B visibility functions from which they are derived have been calibrated identically.

3.3. New mapping method for astrometry of close source pairs

While the conventional phase-referencing approach worked well for our November 1995 observations of 1038+52A and B, the method relies on making a good estimate of the antenna residuals from just one of the sources - the reference. We have devised an alternative method which extends the standard VLBI self-calibration procedure to work on both sources together, for

cases where they have been observed simultaneously, and when either could be used as the reference (see Appendix A).

The basis of the new method is to recognise that, since the visibility functions for both sources are corrupted by the same (antenna-based) phase and phase derivative errors, the sum of the two visibilities also suffers the same errors. We form the point-by-point sum of the two data sets, creating a new one which represents the visibility function of a "compound source" consisting of a superposition of the two structures, corrupted by the common antenna phase errors. If the source separation is close enough, the (summed) data as a function of the (averaged) uv-coordinates can be Fourier Transformed to form a map of the compound source structure, and (iterative) self-calibration in FRING or CALIB yields the antenna-based residuals. The advantage of this approach is that the antenna-based residuals are determined using both source structures simultaneously, and may thus reduce the chance that reference source structural phase terms contaminate the residuals. We term this process "Hybrid Double Mapping" (HDM); a detailed description is given in Porcas & Rioja (1996).

It is convenient to shift the source position in one of the data sets (by introducing artificial phase corrections) prior to the combination into a compound-source data set, to avoid superposition of the images in the map. The phase self-calibration steps which are then applied to the combined data set are identical to the case of a single source. In HDM the information on the angular separation between the sources is preserved in the process of self-calibration of the combined visibilities, and can be measured directly from the compound-image map; the relative positions between the individual source images in the compound map, taken together with any artificial position shift introduced, give the error in the assumed angular separation in the correlator model. In this approach one must be careful to use the same number of visibility measurements in each time interval from the two data sets, in order to avoid the predominance of data from a particular source.

Fig. 3 shows the HDM map of quasars A and B in 1995.9 at λ 3.6 cm; the B source is artificially offset by -4 mas in declination. The rms noise in the map is 0.82 mJy beam^{-1} - higher than that in the hybrid map of B but lower than in that of A.

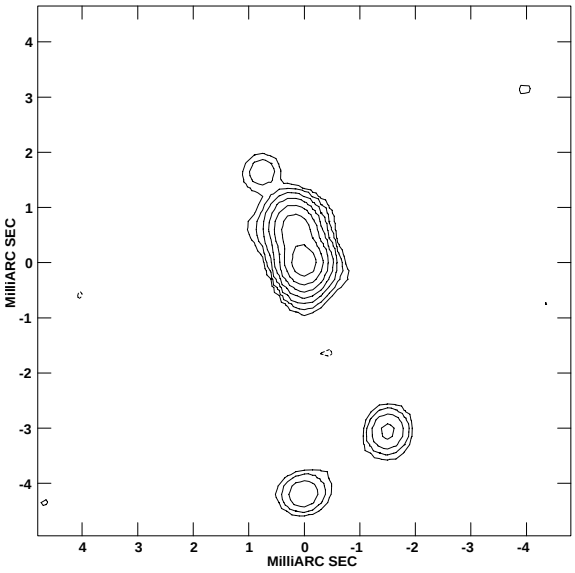

Fig. 3. HDM map of 1038+52 (A+B). Map parameters as in Fig. 1. Quasar B has been offset by -4.0 mas in declination. Contours at 3,6,12,24... mJy beam^{-1}.

4. Analysis of the maps

4.1. Source structures

The 1995.9 hybrid maps of quasars A and B at λ 3.6 cm (Fig. 1) show the core-jet structures typical of quasars at mas scales. They may be compared with maps from previous epochs given in Rioja et al. (1997a). The structure of A in the new map shows no major changes with respect to previous epochs. There is a prominent peak at the SW end of the structure (the "core") and a jet extending in PA 15–25° containing at least two "knot" components (k1 and k2).

The new map of B at 3.6 cm is qualitatively similar to those from previous epochs. It shows 2 point-like components separated by just under 2 mas in PA 127°. Spectral arguments support the identification of the NW component as a "core" (Marcaide & Shapiro 1984); the SE component, corresponding to a knot in the jet, has been used as a reference component in previous astrometric studies. The separation between these 2 components in 1995.9 has increased, continuing the expansion along the axis of the source, as discovered from previous epochs of observations at this wavelength (Rioja et al. 1997a). There is no trace of the third, extreme SE component, seen in maps of this source at 13 cm. This feature is evidently of lower surface brightness at 3.6 cm and is resolved out at the resolution of these observations.

We used AIPS task IMSTAT to estimate total flux densities for quasars A and B (within windows surrounding the sources in the hybrid maps). The values are given in Table 1. Table 1 also lists the fluxes and relative positions of the most prominent features in the maps of A and B, obtained using task JMFIT to find parameters of elliptical Gaussian functions which best fit the various source sub-components. The formal errors from the fits, however, do not give realisitic values for the parameter uncertainties. The distribution of flux between the core and k1 in quasar A, and their relative separation, are quite uncertain, for example.

4.2. Estimating positions of reference features

The astrometric measurement of a separation between two non-point sources must always refer to the measured positions of reference points within maps (or other representations) of the source structures. The selection of suitable reference points is crucial in monitoring programs, where the results from the analysis of a multi-epoch series of observations are compared. Ideally, a reference point should correspond to the peak of a strong, unresolved component, which is well separated from other radio emission within the source structure.

Table 1. Parameters derived from the Hybrid Maps of 1038+528 A and B.

	S-tot (mJy)		S-pk (mJy/b)	S-int (mJy)	maj. (mas)	min. (mas)	PA (deg)	sep. (mas)	PA (deg)
1038+528 A	603.0	core	301.6	355.3	0.28	0.12	3	-	-
		k1	171.8	235.5	0.42	0.16	13	0.639	15.1
		k2	9.3	14.0	-	-	-	1.796	24.8
1038+528 B	86.5	core	33.5	40.9	0.32	0.11	132	-	-
		ref	24.6	34.4	0.39	0.24	123	1.869	127.1

For the 1995.9 epoch observations of 1038+528 A,B we selected the same reference features as those used for the analyses of previous observing epochs. These are the "core" component for quasar A, and the prominent SE component for quasar B. These features are labelled with a cross in Fig. 2a and b. The core of A is indeed strong and compact, but has the disadvantage that it merges with knot k1. Although the SE component of B is no longer the strongest feature at 3.6 cm, it has always been strong at both 3.6 and 13 cm wavelengths, is reasonably compact and is easily distinguishable in maps made at longer wavelengths, thus facilitating spectral studies. Our astrometric analysis refers to the measured positions of the peaks of these components in A and B. We used the AIPS task MAXFIT to measure the position of these peaks in the PRA and HDM maps. MAXFIT defines the location of a peak in a given map region by fitting a quadratic function to the peak pixel value and those of the adjacent pixels. A comparison of this method of defining the peak position with that used for earlier epochs is described in the next section.

4.3. Position error analysis

An analysis of errors presented in Rioja et al. (1997a) shows that the dominant uncertainty in the astrometric measurements of the separation between this close pair of quasars comes from the limited reproducibility of the reference point positions in the VLBI maps, from epoch to epoch. The magnitude of this effect is hard to quantify, however, since it depends on the nature of the source brightness distribution surrounding the reference point, and the method used to define the position of the peak, in addition to the resolution of the array and the signal-to-noise ratio of the peak in the map.

A rough estimate of the error due solely to finite signal-to-noise in the maps is given by dividing the beam size by the ratio of the component peak to the rms noise level in the maps (see e.g. Thompson et al. 1986). This yields values of 3.3, 3.5 and 1.4 μas for the A and B PRA maps and the HDM map. These may be taken to represent lower limits to the reference point position errors; realistic errors will be larger, and will depend on the nature of the reference features and the manner in which the position is estimated.

It is important to choose a definition of the reference point position such that it can be reproduced reliably from epoch to epoch, and is as independent as possible from the parameters used in making the map (e.g. cell size and beam width). The AIPS task JMFIT can be used to fit an elliptical Gaussian to a component in a CLEAN map, for example. However, the position of the peak of the Gaussian depends on how asymmetric the component brightness distribution is, and the area of the map to which the fit is restricted. MAXFIT fits just to the local maximum around the peak map value, and is thus less sensitive to the rest of the distribution.

We have attempted to quantify some limits to reproducibility arising from the use of MAXFIT for defining the peak position in CLEAN maps. We investigated the effect of changing the true position of a point-like source with respect to the pixel sampling (here 3.3 pixels per beam) by offsetting the source position in 10 increments of 1/10 of a pixel in the visibility domain, mapping and CLEANing the new data sets, and estimating the new positions in the CLEAN maps using MAXFIT. The maximum discrepancy found between the values of the artificial offset and the shift derived by MAXFIT was 1/20 of a pixel. This corresponds to 8 μas in our 3.6 cm maps.

For the analysis of previous observing epochs, the reference points were defined to be the centroid of the most prominent delta functions from which the CLEAN source map was derived (Rioja et al. 1997a). We examined possible systematic differences resulting from these different definitions of reference points. One might expect the largest discrepancies to arise when the underlying source structure near the reference point is asymmetric, as in quasar A. We investigated such differences by determining "centroid" positions for both A and B reference components, using various criteria for excluding clean components from the calculation; this included the "25 percent of the value at the peak" threshold used for earlier epochs. For A the difference between this centroid position and the MAXFIT value was 0.12 pixel (18 μas). For B the difference was less than 0.1 pixel. These are probably the largest potential sources of error arising from using different methodologies at different epochs.

Our use of two different mapping procedures - phase-reference mapping and HDM - also gives some insight into the size of position errors resulting from standard CLEAN + phase self-cal mapping algorithms. The differences between the separation estimates from the PRA maps and the HDM map are 27 and 28 μas in RA and Dec respectively. This would suggest that differences in the positions of peaks in maps reconstructed in different ways may vary at the 14 μas level.

Table 2. Change in the separation between quasars A and B in 1995.9 with respect to 1981.2, estimated using standard phase referencing (PRA) and hybrid double mapping (HDM) techniques.

$\Delta(\Delta\alpha)\cos\delta_A$ [μas]	$\Delta(\Delta\delta)$ [μas]	Method
-148	249	PRA
-175	277	HDM

Table 3. *Fixed* source coordinates used for quasar A in the astrometric analysis (these coordinates correspond to GSFC global solution GLB831 (Chopo Ma, priv. comm.)), and separation between quasars A and B measured in 1995.9.

Coordinates	**RA** (J2000)	**DEC** (J2000)
Reference Source **(A)**	$10^h\ 41^m\ 46\overset{s}{.}781613$	$52^0\ 33'28\overset{''}{.}23373$
Relative Sep. **(B-A)**	$2\overset{s}{.}1160588$	$27\overset{''}{.}376325$
Estimated error **(B-A)**	$\pm 0\overset{s}{.}0000027$	$\pm 0\overset{''}{.}000025$

After considering the various possible effects which can limit the accuracy of position estimates, we adopt a "conservative" value for the error in estimating the peak position in our λ 3.6 cm maps, embracing all the effects detailed above, of 18 μas (this corresponds to a thirtieth of the CLEAN beam). The associated estimated error for a separation measurement between the two sources is 25 μas.

4.4. Astrometry results

Table 2 lists the results of our astrometric measurements of reference point positions in the maps. They are presented as changes in measured separation between the reference points in A and B in 1995.9, with respect to their separation in 1981.3. The values given from the phase-reference technique correspond to the difference between the A and B reference feature position offsets in their respective PRA map. The values derived from HDM have been corrected for the artificial offset introduced before adding the A and B source visibilities.

All these values have been corrected for a small error in the AIPS calculation of the u,v coordinates in the frequency-averaged data set. (Distances measured within the maps must be adjusted by a small correction factor of $1 - \Delta\nu * (2\,\nu)^{-1} = 0.998$.)

Table 3 lists the coordinates of the reference source (A) adopted in the analysis and the measured coordinate separation between quasars A and B in 1995.9.

5. Comparison of astrometry at all 4 epochs

In this section we make a comparison of the astrometric measurements from the series of 4 epochs of observations. Any increase of the temporal baseline in the program of monitoring the separation between A and B should result in a more precise identification of any systematic trends, with an improved elimination of random contributions. In Sect. 5.1 we justify comparing the astrometric values measured at the various epochs, even though non-identical observing, post-processing and analysis procedures were involved. In Sect. 5.2 we present the astrometric results from the 4 epochs. In Sects. 5.3, 5.4, 5.5 and 5.6 we present various analyses of these results, and attempt to quantify, or put upper-limits to, proper motions within and between the A and B quasars.

5.1. Comparison between the techniques used at different epochs

Before attempting a comparison of the astrometric results from the 4 observing epochs, we need to show that any bias in the astrometric estimates introduced by the use of different procedures is small compared with other errors in the measurements for the individual epochs. The consistency between the results from previous epochs of observations has been exhaustively tested (Marcaide et al. 1994; Rioja et al. 1997a). We outline here the largest changes involved in the fourth epoch, 1995.9, with respect to previous ones:

1. The observing array and frequency set-up used in the fourth epoch was different from previous epochs of observations (frequency range 8404.5 to 8436.5 MHz instead of 8402.99 to 8430.99 MHz at first 3 epochs). This results in a different coverage of the *UV* plane, leading to changes in the reconstruction of the source images. Investigations of such effects by Marcaide et al. (1994) show that the effect on the astrometric anaylsis is only a few μas. It is important to note that the observations at all 4 epochs have comparable resolutions and sample the same range of structural scales in the sources.
2. The processing of the fourth epoch was done using the VLBA correlator, which uses a theoretical model derived from CALC 8.2; we used AIPS to analyse the data with visibility phases residual to that model. For previous epochs the correlation was done at the MPIfR (Bonn) MK3 correlator, and an analysis of the data using total phases was made with VLBI3 (Robertson 1975). The differences between CALC 8.2 and the one implemented in VLBI3 propagate into changes of only 1-2 μas in the astrometric analysis of the 1038+528 A-B separation (Rioja 1993, Rioja et al. 1997a). This is because any such differences are "diluted" by the source separation expressed in radians - 10^{-4} in the case of this very close source pair.
3. The values used in the analysis of previous epochs for Earth Orientation Parameters (EOP), stations and reference source coordinates were consistently derived from a single global solution provided by Goddard Space Flight Center (GSFC). For the correlation of the fourth epoch, the values used for EOP were derived from IERS solutions, and the station coordinates from USNO catalogs. We have made a comparison of the values derived for all the parameters at the 4 epochs from a single global solution from IERS (namely IERS eopc04), with the actual values used in the individual

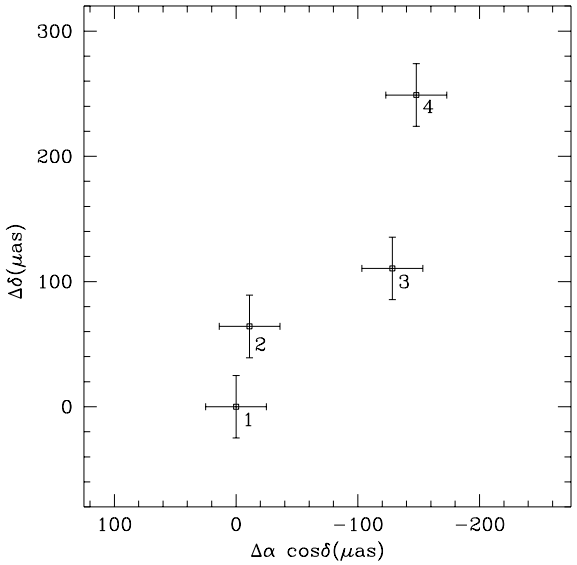

Fig. 4. Measured separations between the A and B reference points at epochs 2 (1983.4), 3 (1990.5) and 4 (1995.9), with respect to epoch 1 (1981.2). Plotted error bars correspond to 25 μas.

epoch analysis. The difference between the corresponding EOP values is always less than 4 mas. Such discrepancies propagate into errors in the relative position estimates at each epoch of only a few μas.

4. Our astrometric analysis in AIPS using a phase-referencing approach and HDM differs from the phase difference method used in VLBI3 analysis. Comparisons show that these procedures are equivalent (Porcas & Rioja 1996; Thompson et al. 1986). Both involve the definition of reference points in source maps; uncertainties in the reference point positions (as described in Sect. 4.3) arise in the same way.
5. Finally, a minor VLBA correlator error (Romney priv. comm.) caused incorrect time labels to be attached to the visibility records, resulting in incorrect (*u*,*v*) values. The effect on the relative visibility phases for our source pair is small ($\sim 0.004°$) and can be neglected.

The magnitudes of all of the effects reported in this section are much smaller than our estimate in Sect. 4.3 of the uncertainity in reproducing the reference point in the source, from epoch to epoch, and we are thus justified in comparing the astrometric results from all 4 epochs.

5.2. Astrometric separations at the 4 epochs

The astrometric measurements of the separations between the reference points in A and B at λ 3.6 cm from 4 epochs are presented in Fig. 4. It includes our new 1995.9 measurement and those from three earlier epochs, in 1981.3, 1983.4 and 1990.5, reported in Marcaide & Shapiro (1984), Marcaide et al. (1994) and Rioja et al. (1997a), respectively. The origin of the plot represents the separation at epoch 1.

Changes with time in Fig. 4 represent the vector difference between any motions of the reference points in quasars A and B. The near-orthogonal nature of the source axes in 1038+52 A,B (along which one might expect any motion to occur) simplifies the interpretation of any trends seen. The new 1995.9 value follows the same steady trend towards the NW shown by the three previous epochs. Rioja et al. (1997a) interpreted this as an outward expansion of the reference component in quasar B at a rate of 18 ± 5 μas yr^{-1}, and quoted an upper bound on any proper motion of quasar A of 10 μas yr^{-1}.

5.3. Vector decomposition

In this section we attempt to separate the individual contributions from the 2 quasars in the astrometric separation measurements presented in Fig. 4. We make no assumption about the stability of either component, but assume that any displacements of the A or B reference points from their positions at epoch 1 are along the corresponding source axis directions. This is a plausible assumption if the reference point coincides with a non-stationary component moving along a ballistic trajectory, or with the location of the peak of brightness within an active core or near the base of jet, where changes during episodes of activity are likely to occur along the jet direction. This approach is closely related to that used previously by Rioja et al. (1997a). For fixed assumed source axes for A and B, it results in a unique decomposition of the changes in the A-B separation into separate A and B displacements, from 1981 to 1995.

It is clear that the dominant contribution to the separation changes seen in Fig. 4 comes from quasar B, in which the source axis is well defined by the 127°PA of the separation between core and reference components. For quasar A the source axis bends, from the inner "core" region (PA = 15°) to the outer jet components, and it is not so clear which direction should be chosen.

In our analysis we tried a range of values for fixing the A source axis (0 to 45° in steps of 5°). For each, we calculated A and B reference-point displacements at epochs 2, 3 and 4 with respect to epoch 1. Then we performed a least-squares fit to the B displacements with time to estimate a linear expansion rate for the B reference feature along PA 127°. In Fig. 5 we plot the deconvolved B reference point displacements from the analysis with the A source axis fixed at PA 25°(the value adopted by Rioja et al. 1997a). The fitted expansion rate is 16.9 ± 0.6 μas yr^{-1}; the error and associated rms values take account of the small number of points and 2 degrees of freedom. This rate agrees well with the value of 18 ± 5 μas yr^{-1} deduced by Rioja et al. (1997a). The rms residual from the fit (7 μas) is low, and vindicates our use of measurements derived from differing techniques for investigating the relative proper motion between A and B.

5.4. Structural evolution within 1038+528 B

Our deconvolution analysis of the changes in separation measured between all 4 epochs supports the finding, previously pro-

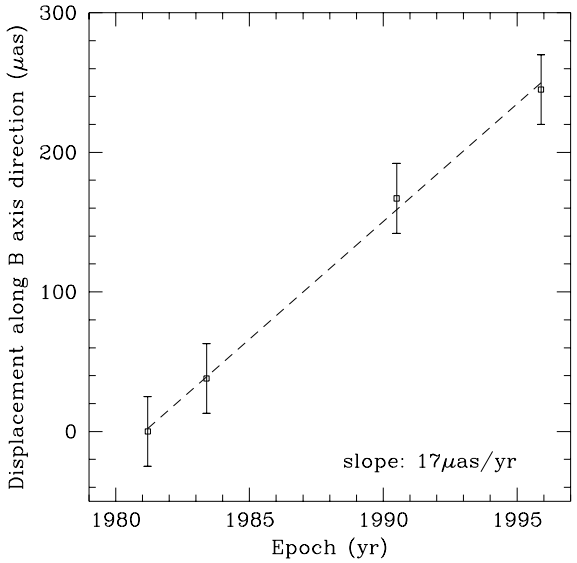

Fig. 5. Changes in position of reference component in B along PA 127°, deduced from deconvolution of the A-B separation measurements. Assumed source axis for A is 25°. Plotted error bars correspond to 25 μas.

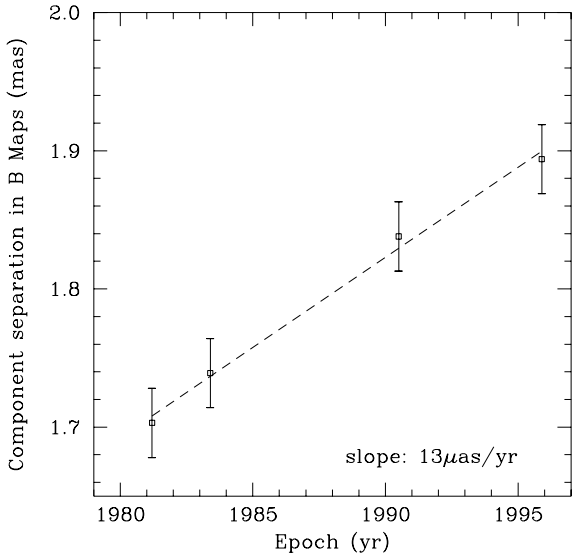

Fig. 6. Changes in the position of the reference component in B along PA 127°, from measurements of its separation from the core in hybrid maps of B. Plotted error bars correspond to 25 μas.

posed, that the B reference component moves along the source axis, away from the B core. In this section we make an independent determination of the separation rate between the core and reference component in B from measurements within the maps at the 4 epochs.

Fig. 6 shows the separation between the core and reference component in B at the four epochs plotted against time. For epochs 1–3 we used the values given in Rioja et al. (1997a). For 1995.9 we used AIPS task UVFIT to estimate a separation from the B visibility data directly, in order to follow the methodology used for the other epochs as closely as possible; the value obtained was 1.895 mas. The slope from a least-squares fit corresponds to an expansion rate of 13.0 ± 0.7 μas yr^{-1}. In the standard picture of extragalactic radio sources, the "core" is stationary, so this corresponds to an outward expansion of the reference component along PA 127°.

The rms of the fit (8 μas) is again surprisingly low, implying typical errors in the separation measurements at each epoch (both within the B structure and between the reference points) of only about 10–12 μas along the direction of the B source axis. This is considerably less than the estimate of position separation errors given in Sect. 4.3.

5.5. Relative proper motion

The analysis presented in the previous sections demonstrate clearly that the chosen reference component within quasar B is unsuitable for use as a marker for tracing any relative proper motion between quasars A and B. The value of its expansion velocity derived in Sect. 5.4 appears to differ significantly from that deduced by vector-decomposition in Sect. 5.3. Although the difference between these estimates, if real, could be interpreted as motion of the core of B at a rate of ~ 4 μas yr^{-1}, this is not a conclusive result since differences of this order arise from choosing different values of PA for the motion in A in the vector decomposition method.

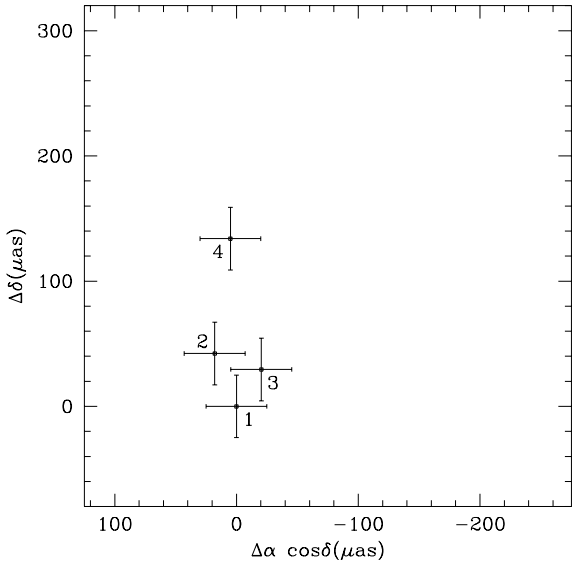

Fig. 7. Separation between the cores of A and B (with respect to epoch 1), derived by correcting the A-B reference point separation measurements with the core-reference separations measured in the B hybrid maps. Plotted error bars correspond to 25 μas.

A more suitable tracer of relative proper motion between the quasars is the variation of the separation between the cores of A and B. We have used the separations between the core and reference component measured in the B map at each epoch, and the astrometric separations between A and B, to calculate the separations between the A and B cores at each epoch; these are plotted in Fig. 7. The area occupied by the points defines an upper limit of ~ 10 μas yr^{-1} for any relative proper motion

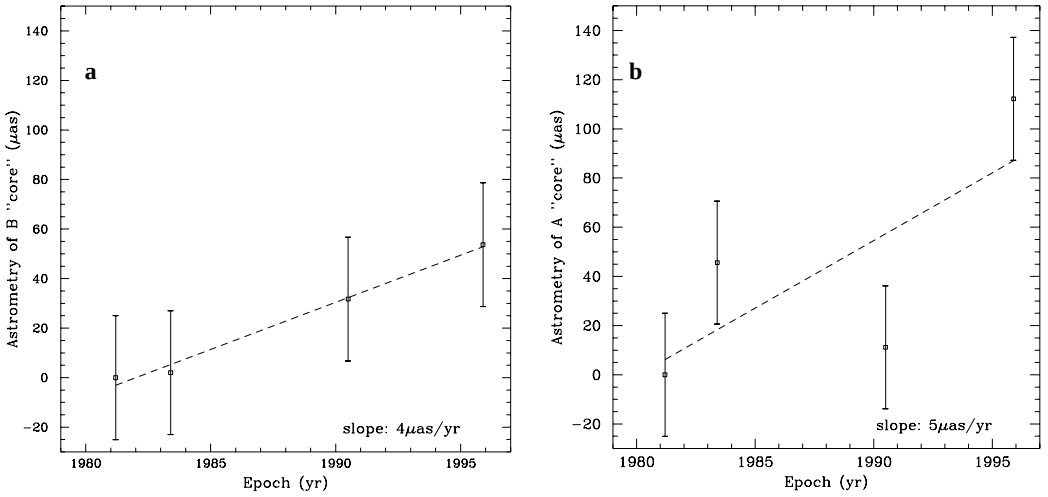

Fig. 8a and b. Residual motions of the cores using the deconvolution approach. **a** Displacements of B core along PA 127°; **b** Displacements of A core along PA 25°. Plotted error bars correspond to 25 μas.

between the A and B cores, and hence between the quasars themselves, during the period of nearly 15 years for which the separation has been monitored with VLBI. The limit seems to be set by the relatively large deviation of the 1995.9 epoch point in the direction of the A source axis, presumably arising from the difficulty in defining the reference point at the A "core" from epoch to epoch.

5.6. Possible "core" motions?

Finally, we investigate any possible residual motions of the "cores" in A and B. The most likely causes of any such apparent motions are changes in the relative brightness or positions of features in the source structures at a resolution below that of the maps. One might expect that these, too, would produce effects predominantly along the source axis directions. We therefore used the vector deconvolution method on the plot of core-core separation with time to study displacements of the cores along their source axis directions. Fig. 8a and b show plots of the separated contributions from B and A, for an assumed A source axis PA 25°. The displacements for the B core seem to increase systematically. The fitted rate is 3.8 ± 0.3 μas yr^{-1}, indicating a possible slow outward motion. The displacements for the A core do not seem to vary systematically - the fitted slope is 5.5 ± 3.6 μas yr^{-1}. Here the scatter is considerably larger, reflecting both the difficulties of defining the reference point along the A core-jet axis, and also, perhaps, real "jitter" of the position of the peak due to variations in the "core" substructure. These plots indicate the level of stability of the individual core positions; the fits represent realistic upper limits to any possible systematic core motion in the A and B quasars along their source axis directions.

6. Conclusions

The series of astrometric VLBI measurements of the separation between the quasar pair 1038+528 A and B, spanning nearly 15 years, provides excellent material for investigating the relative proper motion of two extragalactic radio sources and the positional stability of their cores. The changes measured in the separations between quasars A and B at 3.6 cm are dominated by the motion of the reference feature in quasar B. These astrometric results, and measurements in the hybrid maps of B are compatible with an expansion rate for the B reference component of 13–17 μas yr^{-1}. At a redshift of 2.296 this translates to an apparent transverse velocity of 0.55–0.70 c h^{-1}. We note that this is an order of magnitude smaller than the more typical superluminal velocities seen in many quasars; it is a rare example of a subluminal velocity measured for a knot in a quasar jet.

After correcting for the motion of the reference component in B, we can put a conservative upper bound to any relative proper motion between the quasars of 10 μas yr^{-1}. Despite the increase in temporal baseline, this upper bound is no better than that given by Rioja et al. (1997a). Its value is related to the difficulty in reproducing a stable reference position along the A source axis near its "core".

Theories in which the redshifts of quasars do not indicate cosmological distances, and in which quasars are "local" and have high Doppler redshifts (e.g. Narlikar & Subramanian 1983) are incompatible with our measured upper-limit to relative proper motion. Quasars at 100 Mpc distance moving at relativistic speeds would have proper motions of the order of 600 μas yr^{-1}, nearly 2 orders of magnitude greater than our limit. Assuming cosmological distances, our limit corresponds to apparent transverse velocities of 0.43 c h^{-1} and 0.22 c h^{-1} at the redshifts of the B and A quasars, respectively.

We have investigated the way in which the definition of reference points in a map may be only loosely "fixed" to the radio source structure, especially when the latter is strongly asymmetric. We have also developed an alternative analysis route - Hybrid Double Mapping - for imaging both sources of a close pair simultaneously, and at the same time preserving their relative astrometric information in a single map.

The surprisingly low rms from the fits of linear expansion in quasar B, and the discrepancy between the two estimates (16.9 ± 0.6 μas yr^{-1} from the astrometric measurements and 13.0 ± 0.7 μas yr^{-1} from the hybrid maps) are suggestive of (but do not prove) a residual motion of the core in quasar B;

our decomposition along the source axis direction gives a fit of 3.8 ± 0.3 μas yr^{-1}, corresponding to an apparent transverse velocity of 0.17 c h^{-1}. If real, this might indicate a steady change in physical conditions at the base of the jet, or perhaps the emergence of a new knot component moving outwards with a velocity similar to the reference component, but as yet unresolved by our 0.5 mas beam. In this regard, it is interesting to note the slight extension of the core of quasar B in PA 132° given by the Gaussian model fit.

The low rms derived from fits to the expansion of the B reference component indicate that we have been overly conservative in our estimate of 18 μas for the error in reference point positions. Errors at least 2 times smaller are implied, corresponding to a sixtieth of the beamwidth. It is interesting to note that such small errors are also implied in the work of Owsianik & Conway (1998), where the low scatter in the plot of expansion of the CSO source 0710+439 allows an expansion rate of 14.1 ± 1.6 μas yr^{-1} to be determined.

There are no obvious systematic motions within quasar A, but the "noise" in the estimates of position along its axis are much larger. This noise, along with any associated underlying changes in source substructure, provides a fundamental limit to estimates of any systematic core motion in A. Improvements on the estimates of (or upper bounds to) the relative motion between the quasars, or of the individual motion of the A core, will require a considerable increase in the temporal baseline of VLBI monitoring.

Appendix A: Hybrid Double Mappping (HDM)

A.1 Principle of Hybrid Double Mapping

The visibility function, V, measured at time t, on a baseline between antennas i and j, is represented by a complex function with amplitude A, phase P:

$$V(i,j) = A * e^{i[\phi]}(t)$$

For this analysis it is convenient to indentify 3 contributions to the visibility phase:

$$\phi(i,j) = \phi_s(u,v) + \phi_p(u,v) + \phi_m(t)$$

where

- ϕ_s is due to source structure, evaluated w.r.t. a reference position for the source.
- ϕ_p is due to any offset of the true source position from the reference position.
  Both ϕ_s and ϕ_p are functions of the resolution coordinates, u and v, at time t.
- ϕ_m is due to inaccuracies in the correlator model calculation of the interferometer geometry and the signal propagation delays in the ionosphere, troposphere and receiving system; it is an unknown function of time.
  This term can be represented by the difference of two "antenna-based" phases, θ_i and θ_j, since it can be related to the difference in signal arrival times at the two sites. (This analysis is a simplification which ignores possible "non-closing" instrumental baseline phase terms arising from e.g. un-matched bandpasses and polarisation impurities.)

$$\phi(i,j) = \phi_s(u,v) + \phi_p(u,v) + \theta_i(t) - \theta_j(t)$$

In conventional hybrid mapping, an iterative procedure is used to separate out the antenna-based phase terms from the "source" terms; the latter must produce a consistent and physically plausible source structure after Fourier transformation of the corrected visibility:

$$\underbrace{A * e^{i[\phi_s+\phi_p]}(u,v)}_{corrected\ visibility} = V(i,j) * \underbrace{e^{-i[\theta_i(t)-\theta_j(t)]}}_{antenna\ phase\ terms}$$

However, the position offset term, ϕ_p, can also be expressed as a difference in wavefront arrival times at the 2 antennas and so it is also "absorbed" in antenna phase terms θ'_i, θ'_j; the "absolute" position information is lost:

$$\underbrace{A * e^{i[\phi_s]}(u,v)}_{corrected\ visibility} = V(i,j) * \underbrace{e^{-i[\theta'_i(t)-\theta'_j(t)]}}_{antenna\ phase\ terms}$$

In Hybrid Double Mapping (HDM), the visibility functions of two sources observed simultaneously are added. For a close source pair, we make the same assumption as for conventional phase-referencing - that the model error phase terms are essentially the same for both sources. We make a further assumption that the u, v coordinates are also essentially the same for both sources, for each baseline and time. The visibility sum, V^1+V^2, can then be re-written:

$$\underbrace{(A^1 * e^{i[\phi^1_s]} + A^2 * e^{i[\phi^2_s+(\phi^2_p-\phi^1_p)]})(u,v)}_{corrected\ visibility\ sum} =$$

$$= V^{sum}(i,j) * \underbrace{e^{-i[\theta'_i(t)-\theta'_j(t)]}}_{antenna\ phase\ terms}$$

This may be recognised as the visibility function of a "composite" source consisting of the sum of the brightness distributions of sources 1 and 2, with antenna-based phase error terms θ'_i, θ'_j, as before. The HDM method consists of performing the normal hybrid mapping procedure with the visibility sum, resulting in the separation of the antenna-based errors, and a physically plausible map of the sum of the two source brightness distrubutions. An important point is that, whereas the *origin* of the map of the composite source is arbitrary (as it depends on the position of the starting model), the *separation* of the two source brightness distributions within the composite map (determined by $\phi^2_p - \phi^1_p$) is fixed during the phase separation procedure, and is equal to the *difference* of the errors in the two source positions used for correlation. We call this the "residual separation".

A.2 Practical aspects

There are some practical aspects to be considered. If the source coordinates used in the correlator model are very precise, then

the residual separation may be less than the interferometer beamwidth, and the two source distributions will lie on top of each other. In this case it is desireable to introduce an artificial position offset into one of the source visibility functions before forming the visibility sum, to ensure that the two source reference features are well separated in the HDM map. One should also arrange that the peak of one source does not lie on the sidelobe response of the other in the "dirty" map, as this may degrade the CLEAN deconvolution process in the mapping step.

Another important consideration is that the time-averaged samples of the summed visibility function contain equal contributions from both source visibility functions. When both sources are observed simultaneously this will normally be the case, except when different amounts of data are lost in the two separate correlator passes needed for the two source positions. It is important to edit the data sets carefully to fulfil this condition.

The range of validity of the assumption that the (u, v) coordinates for the two sources are the same depends on the "dilution factor", i.e. the reciprocal of the source separation, measured in radians. The (u, v) value assigned to the summed visibility will be incorrect for either source by roughly 1 part in the dilution factor (roughly 1 in 6000 for 1038+528A,B). This is equivalent to having source visibility phase errors of this order, and thus limits the size of an HDM map to be less than the beamwidth times the dilution factor; the residual separation should be much smaller than this value.

In the actual analysis used in this work, we first made a rough correction to the phase of the summed visibility of 1038+528 A + B, using the antenna phase and phase derivative errors from fringe-fitting 1038+528A using a point source model. However, there is no reason why one should not fringe-fit the summed visibility function directly.

A.3 Applications

The HDM method can in principle be applied whenever two (or more !) radio sources are observed simultaneously, but are correlated at separate field centres; however, they must be close enough so that the conditions of same (u, v) coverage and same correlator model errors apply. The method uses the structures of BOTH sources simultaneously to separate out the antenna phase errors, as opposed to a single source in simple hybrid mapping. If both sources are strong (as with 1038+528 A and B), constraining the (single) antenna phase solutions with two structures should lead to a more rigorous and robust separation between the source and antenna phase terms. One field of application is in high resolution VLBI imaging of gravitational lens systems with wide image separations (e.g. images A and B of QSO 0957+561 with 6.1 arcsec separation) where preserving the necessary wide field-of-view from a single correlation may result in inconveniently large data sets. When one source is very weak, however, there is probably little to be gained over normal hybrid mapping.

For relative astrometry studies (as described in this paper), the HDM method has some advantages over conventional phase-reference mapping and explicit phase-differencing methods. In phase-differencing astrometry, separate hybrid maps must be made of both sources to correct for source structural phase terms and the antenna phase errors are NOT constrained to be the same. Imperfect separation between source and antenna phase terms can increase the noise on the differenced phase, as well as lead to possible systematic errors. In phase-reference astrometry, only one of the sources is used to solve for the antenna phase terms; imperfect separation can lead to extra phase noise in the phase-referenced visibility of the "target" source. In HDM we use both source structures simultaneously to separate the (common) antenna error phases from that of a single "structure" in which the reference points of the two sources are spaced by the residual separation.

When the separation between the two sources of a pair exceeds the telescope primary beamwidths, astrometric and phase-reference observations must involve switching between the sources, and the visibility phase of at least one of the sources must normally be interpolated in the observing gap. The condition that must be fulfilled for HDM to work in this case is that an equal number of observations of both sources must be added to form an average visibility function for the length of the "solution interval" in the phase self-calibration step of HDM. This length is generally limited by the coherence time of the atmosphere, and would imply a very fast switching cycle in most cases. Another application for HDM could be in the the analysis of "cluster-cluster" VLBI (see e.g. Rioja et al. 1997b), in which two or more sources are observed simultaneously on VLBI baselines by using more than one telescope at each site.

Acknowledgements. We thank Dave Graham for help with the observations in Effelsberg, Tony Beasley for asistance at the VLBA, and Mark Reid for useful comments on the text. M.J.R. wishes to acknowledge support for this research by the European Union under contract CHGECT920011. The National Radio Astronomy Observatory is a facility of the National Science Foundation operated under cooperative agreement by Associated Universities, Inc.

References

Alef W.A., 1988, In: Reid M., Moran J. (eds.) Proc. IAU Symp. 129, Kluwer, p. 523
Beasley A.J., Conway J.E., 1995, In: Zensus J.A., Diamond P.J., Napier P.J. (eds.) Very Long Baseline Interferometry and the VLBA. ASP Conference Series Vol. 82, p. 327
Blandford R.D., Königl A., 1986, ApJ 308, 83
Marcaide J.M., Shapiro I.I., 1983, AJ 88, 1133
Marcaide J.M., Shapiro I.I., 1984, ApJ 276, 56
Marcaide J.M., Elósegui P., Shapiro I.I., 1994, AJ 108, 368
Narlikar J.V., Subramanian K., 1983, ApJ 273, 44
Owen F.N., Porcas R.W., Neff S.G., 1978, AJ 83, 1009
Owen F.N., Wills B.J., Wills D., 1980, ApJ 235, L57
Owsianik I., Conway J.E., 1998, A&A 337, 69
Porcas R.W., 1987, In: Zensus A., Pearson A. (eds.) Superluminal Radio Sources. Cambridge University Press, p. 12

Porcas R.W., Rioja M.J., 1996, In: Elgered G. (ed.) Proc. of the 11th Working Meeting on European VLBI for Geodesy and Astrometry, p. 209
Rioja M.J., 1993, Ph.D. Thesis, Universidad de Granada
Rioja M.J., Marcaide J.M., Elósegui P., Shapiro I.I., 1997a, A&A 325, 383
Rioja M.J., Stevens E., Gurvits L., et al., 1997b, Vistas in Astronomy 41 (2), 213
Robertson D.S., 1975, Ph.D. Thesis, MIT
Thompson A.R., Moran J.M., Swenson G.W., 1986, In: Interferometry and Synthesis in Radio Astronomy. Wiley-Interscience, New York, p. 400